Stability Analysis of Bidirectional Dual Active Bridge Converter With Input and Output LC Filters Applying Power-Feedback Control

Yasushi Eto, *Student Member, IEEE*, Yuichi Noge, *Member, IEEE*, Masahito Shoyama, *Senior Member, IEEE*, and Tadatoshi Babasaki

***Abstract*—This article analyzes the dynamic characteristics of a dual active bridge (DAB) converter with input/output LC filters connected and power-feedback control applied, and then discusses an impedance stability criterion about both side LC filters and the converter. Power control is suitable as a control method for grid-connected converters because of its affinity with the energy management system, which is being introduced as a new way to operate power systems in recent years. In order to provide stable power supply, it is necessary to ensure the stability of the converter, and information on dynamic characteristics is essential for the design and development of converters. Since there are no previous papers found yet where the impedance stability criterion is applied when LC filters are connected to both ends of a bidirectional DAB converter, this article discusses the procedures and key points to be considered to apply the criterion. Based on the analysis, the design guidelines of the system will be discussed.**

***Index Terms*—DC microgrid, dual active bridge (DAB) converter, dynamic characteristics, impedance stability criterion, LC filter, power-feedback control.**

I. Introduction

THE introduction of renewable energy sources (RES), such as photovoltaics are actively promoted as a means of addressing environmental issues [1]. In order to promote the use of these renewable energies, microgrid, an independent distribution system, has become a solution for overcoming power fluctuations of renewable energy sources [2]. Among them, dc microgrid (DCMG) becomes attractive since the development of dc–dc conversion technology and growth of electric dc devices [e.g., battery energy storage (BES), photovoltaics, communication facility, computers] [3].

Dc–dc converters are used for power conversion in dc distribution system, which utilize fast switching operation by semiconductor devices [4]. Especially, a bidirectional dc–dc converter, which performs bidirectional power transmission, can be used to connect to a BES that charges and discharges, or to connect DCMGs in which distributed power supplies are installed [5]. For an interconnection of DCMGs, dual active bridge (DAB) converter [6], [7], [8] is suitable as an isolated bidirectional dc–dc converter and it can achieve high efficiency at a heavy load.

At the same time, energy management system (EMS) is another solution of utilizing RES, which monitors the amount of electricity generated and consumed by each power facility for optimal operation of the grid by using communications technology [11], [12]. With increasing social expectations for the Internet of Things and data analysis technology using artificial intelligence, it is expected that EMS will become even more widespread. The control method of dc–dc converters is basically an output voltage control targeting resistive loads [13]. For example, not only a typical voltage-feedback [14], but also a voltage-feedback with output current feedforward compensation [15] and virtual direct power control [16] can be mentioned. However, these voltage control methods cannot transmit the desired power when the dc bus voltage is kept constant by BES or another converter in the DCMG. On the other hand, constant current control is often used to transmit power to a system where the voltage is kept constant, such as BES [17], [18], [19], [20]. One of the concerns with the current control is that accurate power transmission may not be possible if the dc bus voltage deviates from the expected value. As an implementing EMS at interconnected DCMGs, power-feedback control for grid-connected DAB converter may be the best way to transfer a desired power to another grid.

A dynamic model of dc–dc converter is mainly concerned to analyze stability of both converters and DCMGs. The conventional dynamic analysis of DAB converters was mainly based on a circuit model with a voltage source at the input side and a load element at the output side [21], [22], [23], [24], [25], [26], and [27]. But in the situation of dc grid-interconnection, a converter model which regard the dc grid as an ideal dc voltage supply may be considerable because BES in grid maintains a

Manuscript received 28 May 2022; revised 13 August 2022 and 11 October 2022; accepted 15 November 2022. Date of publication 28 November 2022; date of current version 26 December 2022. An earlier version of this paper was presented in part at the 2021 IEEE 12th Energy Conversion Congress & Exposition - Asia (ECCE-Asia) [DOI: 10.1109/ECCE-Asia49820.2021.9479008]. Recommended for publication by Associate Editor F. J. Azcondo. *(Corresponding author: Yasushi Eto.)*

Yasushi Eto is with the Graduate School of Information Science and Electrical Engineering, Kyushu University, Fukuoka 819-0395, Japan (e-mail: eto.yasushi@ieee.org).

Yuichi Noge and Masahito Shoyama are with the Faculty of Information Science and Electrical Engineering, Kyushu University, Fukuoka, Fukuoka 819-0395, Japan (e-mail: noge@ees.kyushu-u.ac.jp; shoyama@ees.kyushu-u.ac.jp).

Tadatoshi Babasaki is with the NTT Facilities Inc, Tokyo 108-0023, Japan (e-mail: babasa23@ntt-f.co.jp).

Color versions of one or more figures in this article are available at https://doi.org/10.1109/TPEL.2022.3225113.

Digital Object Identifier 10.1109/TPEL.2022.3225113

bus voltage constantly. In the previous research in [28] and [29], the small-signal model of DAB converter with input/output LC filters interfacing dc voltage supplies is considered. However, the analysis in [28] and [29] does not include a feedback system. There is another previous work which apply the power-feedback control for DAB converter without LC filters [30], [31], but the dynamic model of power-controlled DAB converters which include LC filters has not yet been studied in detail. A study of the model and characteristics of the system, which has not yet been examined, will enable more efficient design of the system for other engineers to use. Therefore, this article considered the dynamic characteristic of the grid-connected DAB converter with power-feedback control.

Meanwhile, when implementing the converters to the DCMG, it is recommended to add LC filters on the input and output side of the converter to reduce the switching ripple of voltage and current and improve the quality of the power system [32], [33]. The instability caused by the cascade of dc–dc converter and input LC filter has been discussed by [34], and the impedance stability criterion above a single dc bus has been studied [35], [36], [37], [38], [39], [40], [41], [50], [51]. In addition, system design guidelines and stabilization methods based on the criterion were studied [42], [43], [44]. Cespedes et al. [42] discussed input LC filter design guidelines for a constant power load (CPL), and Zhang et al. [44] discussed the LC filter design guidelines connected to the input side of a load converter. Zhang et al. [43] deals stabilization methods in the situation where a source converter is connected to the input stage of a unidirectional load converter. The impedance criterion with the input LC filter under unidirectional power transfer were also considered for a DAB converter [45], [46], [47], [48], and the previous research [28] analyzes the dynamic model of the power stage of the DAB converter when input and output LC filters are connected. However, the abovementioned papers dealing with impedance stability criterion is limited to the situation of unidirectional power transmission, and the influence of both side LC filters on the power-feedback control system is not specifically studied. Therefore, this article also discusses the effect of input and output LC filters to the stability of bidirectional power control system for the DAB converter and the design guidelines of the converter.

This article is organized as follows. At first, this article reviews a basic characteristic of the DAB converter in Section II, and then small signal models and important transfer functions of the DAB converter with power-feedback control are obtained in Section III, which connects input/output LC filters. Section IV discusses a theory and an application procedure of impedance stability criterion for the DAB converter. In Section V, experimental results confirm the validity of small-signal model and the stability analysis results, and Section VI discusses the system design guidelines of the converter with feedback. Finally, Section VII concludes this article.

II. Basic Characteristic of DAB Converter

A schematic without input/output LC filters and a basic waveform of the DAB converter are shown in Figs. 1 and 2, respectively. This converter transmits power in both directions

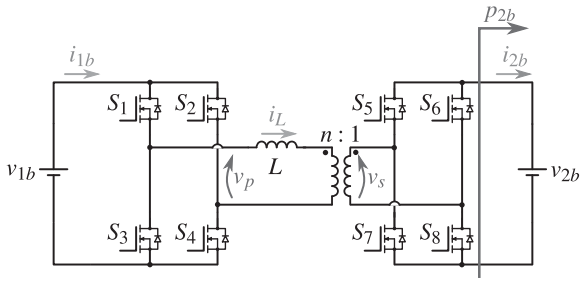

Fig. 1. Schematic of DAB converter interfacing dc voltage supplies.

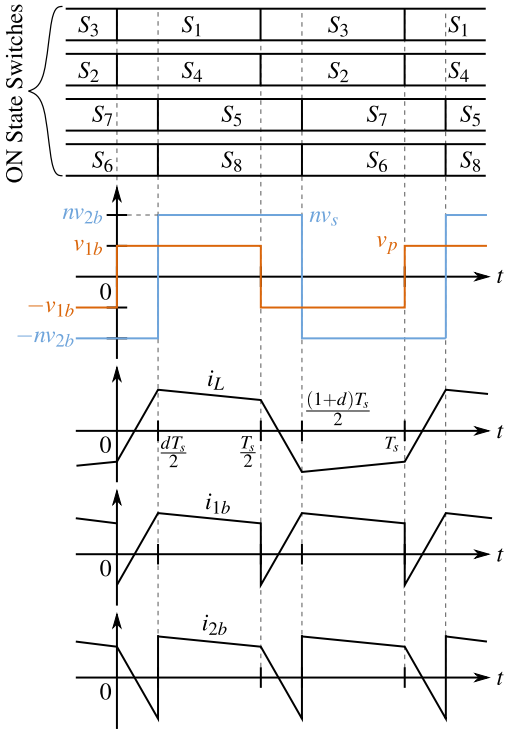

Fig. 2. Basic waveform of DAB converter.

by the phase shift $dT_s/2$ between the square wave voltages v_p and v_s generated from the inverter circuits at both ends. To simplify the stability analysis, DAB converter was assumed to operate single phase shift (SPS) modulation [9] in this article.

The average current $\bar{i}_{1b}, \bar{i}_{2b}$ flowing at both ends of the converter and an average transmission power $\bar{p}_{2b}$ are expressed in (1)–(3), respectively, by assuming voltages v_{1b} and v_{2b} and the phase shift ratio d do not change in time within one cycle, and there is no power loss in the converter. In addition, the function $f(d)$ is defined in (4) to improve the prospect of future equations

$$\bar{i}_{1b} := \frac{1}{T_s}\int_0^{T_s} i_{1b}\,dt = v_{2b}f(d) \tag{1}$$

$$\bar{i}_{2b} := \frac{1}{T_s}\int_0^{T_s} i_{2b}\,dt = v_{1b}f(d) \tag{2}$$

$$\bar{p}_{2b} = \frac{1}{T_s}\int_0^{T_s} p_{2b}\,dt = v_{1b}v_{2b}f(d) \tag{3}$$

$$f(d) = \frac{n}{\omega_s L}\pi d(1-|d|). \tag{4}$$

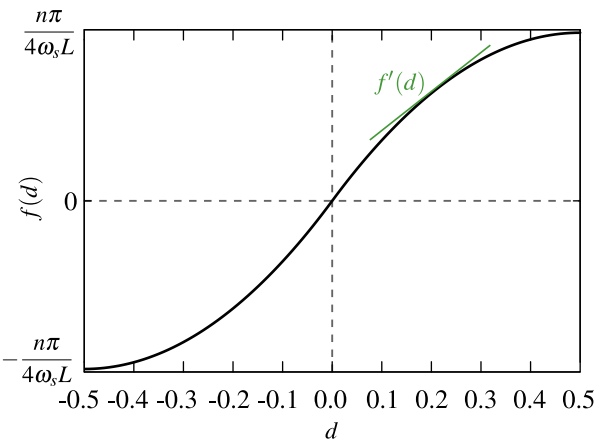

Fig. 3. Graph of $f(d)$.

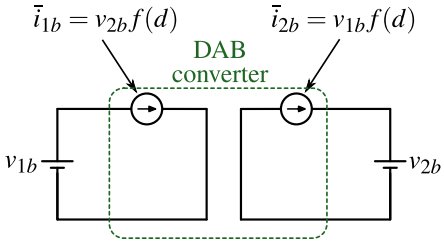

Fig. 4. Averaging model of DAB converter.

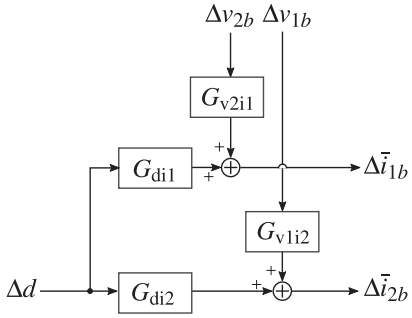

Fig. 5. Small-signal block diagram of DAB converter.

An approximate form of $f(d)$ is shown in Fig. 3. It can be found that the primary side average current $\bar{i}_{1b}$ is not dependent on the primary side voltage v_{1b} from (1), and the secondary side average current $\bar{i}_{2b}$ is not dependent on the secondary side voltage v_{2b} from (2). Therefore, an averaging model of DAB converter can be represented by ideal current sources, as in Fig. 4.

By considering a small-signal perturbation at a dc operating point in (5) and (6), $\Delta\bar{i}_{1b}$ and $\Delta\bar{i}_{2b}$ are derived in (7) and (8), and a dynamic model of the converter can be expressed in Fig. 5

$$v_{1b} \to V_{1b} + \Delta v_{1b}, v_{2b} \to V_{2b} + \Delta v_{2b}, d \to D + \Delta d \quad (5)$$

$$\bar{i}_{1b} \to I_{1b} + \Delta\bar{i}_{1b}, \bar{i}_{2b} \to I_{2b} + \Delta\bar{i}_{2b} \quad (6)$$

$$\Delta\bar{i}_{1b} = G_{v2i1}\Delta v_{2b} + G_{di1}\Delta d \quad (7)$$

$$\Delta\bar{i}_{2b} = G_{v1i2}\Delta v_{1b} + G_{di2}\Delta d \quad (8)$$

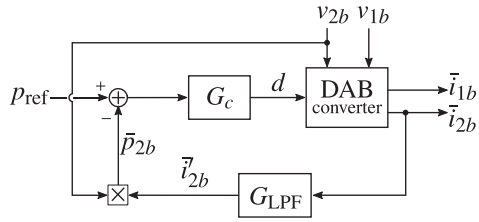

Fig. 6. Block diagram of power-feedback control for DAB converter.

where $G_{v2i1}, G_{di1}, G_{v1i2},$ and G_{di2} are represented in

$$G_{v2i1} = f(D) \quad (9)$$

$$G_{di1} = V_{2b} f'(D) \quad (10)$$

$$G_{v1i2} = f(D) \quad (11)$$

$$G_{di2} = V_{1b} f'(D) \quad (12)$$

and $f'(D)$ is represented in (13) which is the derivative of $f(D)$ by D. The derivation of $f'(D)$ is described in the Appendix

$$f'(D) = f'(d)|_{d=D} = \frac{n}{\omega_s L}\pi(1 - 2|D|). \quad (13)$$

III. Small-Signal Model of Power-Feedback Controlled DAB Converter

A. Small-Signal Analysis Without LC Filters

The block diagram of power-feedback control for DAB converter is shown in Fig. 6. For simplicity, the controller G_c is assumed to be a PI controller with control delay and the low-pass filter G_{LPF} is assumed to be a first-order low-pass filter (1st-LPF) which are represented as follows:

$$G_c = \left(K_p + \frac{K_i}{s}\right) e^{-sT_D} = K_p \left(1 + \frac{2\pi f_i}{s}\right) e^{-sT_D} \quad (14)$$

$$G_{LPF} = \frac{\omega_c}{s + \omega_c} \quad (15)$$

where $K_i = 2\pi f_i K_p$, $\omega_c = 2\pi f_c$, f_c is a cutoff frequency of G_{LPF}, f_i is a corner frequency of the PI controller, and s is the Laplace operator.

From Fig. 6, the phase shift ratio d is represented as

$$d = G_c \left(p_{ref} - v_{2b}\bar{i}'_{2b}\right). \quad (16)$$

By considering small-signal perturbation in (17) and (18), Δd is derived in (19)

$$d \to D + \Delta d, p_{ref} \to P_{ref} + \Delta p_{ref} \quad (17)$$

$$v_{2b} \to V_{2b} + \Delta v_{2b}, \bar{i}'_{2b} \to I'_{2b} + \Delta\bar{i}'_{2b} \quad (18)$$

$$\Delta d = G_c \left(\Delta p_{ref} - V_{2b}\Delta\bar{i}'_{2b} - I_{2b}\Delta v_{2b}\right) \quad (19)$$

where $I'_{2b} = I_{2b}$, and second-order micro terms is neglected.

By using (7), (8), and (19), a small-signal block diagram of the DAB converter with the power-feedback control can be derived, as in Fig. 7. Then, a loop transfer function T_{DAB}, primary side impedance Z_{1b}, and secondary side impedance Z_{2b} are

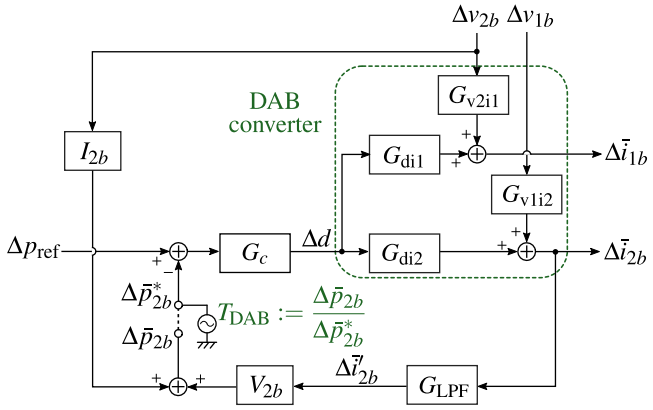

Fig. 7. Small-signal block diagram of the power-feedback system without LC filters.

derived in

$$T_{\text{DAB}} = \frac{\Delta\bar{p}_{2b}}{\Delta\bar{p}^*_{2b}} = -G_c G_{\text{LPF}} G_{\text{di2}} V_{2b} = -G_c G_{\text{LPF}} f'(D) V_{1b} V_{2b} \tag{20}$$

$$Z_{1b} = \frac{\Delta v_{1b}}{\Delta\bar{i}_{1b}} = -\frac{1 + G_c G_{\text{di2}} G_{\text{LPF}} V_{2b}}{G_{\text{v1i2}} G_{\text{di1}} G_{\text{LPF}} V_{2b} G_c} \tag{21}$$

$$Z_{2b} = -\frac{\Delta v_{2b}}{\Delta\bar{i}_{2b}} = \frac{1 + G_c G_{\text{di2}} G_{\text{LPF}} V_{2b}}{G_c G_{\text{di2}} I_{2b}}. \tag{22}$$

This article defined T_{DAB} as a transfer function which the input as $\Delta\bar{p}^*_{2b}$ and the output is $\Delta\bar{p}_{2b}$. In (20), it is found that the order of T_{DAB} is determined by the controller G_c and the low-pass filter G_{LPF} because V_{1b}, V_{2b}, and $\frac{df}{dD}$ are proportional gains. The gain of T_{DAB} mainly depends on the steady-state value of phase shift ratio D, and the stability and responsiveness of the control system are affected by D.

B. Small-Signal Analysis With LC Filters

A schematic of the DAB converter with input/output LC filters are shown in Fig. 8. If the variation of voltage v_{1b}, v_{2b} per cycle is sufficiently small, the averaging model of this converter can be represented, as in Fig. 9.

By solving circuit equations of Fig. 9, transfer functions $G_{\text{v1b}}, Z_{\text{LC1}}, G_{\text{v2b}},$ and Z_{LC2} are derived as

$$\bar{v}_{1b} = G_{\text{v1b}} v_1 + G_{\text{i1b}} \bar{i}_{1b} \tag{23}$$

$$G_{\text{v1b}} = \frac{r_{C1} C_1 s + 1}{L_1 C_1 s^2 + (r_{L1} + r_{C1}) s + 1} \tag{24}$$

$$Z_{\text{LC1}} = -\frac{r_{C1} L_1 C_1 s^2 + (r_{L1} r_{C1} C_1 + L_1) s + r_{L1}}{L_1 C_1 s^2 + (r_{L1} + r_{C1}) s + 1} \tag{25}$$

$$\bar{v}_{2b} = G_{\text{v2b}} v_2 + G_{\text{i2b}} \bar{i}_{2b} \tag{26}$$

$$G_{\text{v2b}} = \frac{r_{C2} C_2 s + 1}{L_2 C_2 s^2 + (r_{L2} + r_{C2}) s + 1} \tag{27}$$

$$Z_{\text{LC2}} = \frac{r_{C2} L_2 C_2 s^2 + (r_{L2} r_{C2} C_2 + L_2) s + r_{L2}}{L_2 C_2 s^2 + (r_{L2} + r_{C2}) s + 1}. \tag{28}$$

And by considering small-signal perturbation in (29) and (30), $\Delta\bar{v}_{1b}$ and $\Delta\bar{v}_{2b}$ are derived in (31) and (32), respectively

$$\bar{v}_{1b} \to V_{1b} + \Delta\bar{v}_{1b}, \bar{i}_{1b} \to I_{1b} + \Delta\bar{i}_{1b}, v_1 \to V_1 + \Delta v_1 \tag{29}$$

$$\bar{v}_{2b} \to V_{2b} + \Delta\bar{v}_{2b}, \bar{i}_{2b} \to I_{2b} + \Delta\bar{i}_{2b}, v_2 \to V_2 + \Delta v_2 \tag{30}$$

$$\Delta\bar{v}_{1b} = G_{\text{v1b}} \Delta v_1 + Z_{\text{LC1}} \Delta\bar{i}_{1b} \tag{31}$$

$$\Delta\bar{v}_{2b} = G_{\text{v2b}} \Delta v_2 + Z_{\text{LC2}} \Delta\bar{i}_{2b}. \tag{32}$$

In order to reproduce the same situation as in the previous section, this article assumes that v_{2b}, i_{2b} in Fig. 8 are detected and the transmission power p_{2b} is controlled. The small-signal model of power-feedback system with LC filters is shown in Fig. 10 by applying (31) and (32) to the block diagram in Fig. 7. A loop transfer function T_{all} in Fig. 10 and a closed-loop transfer function G_p can be derived as

$$T_{\text{all}} = \frac{\Delta\bar{p}_{2b}}{\Delta\bar{p}^*_{2b}} = \frac{-G_c \left(I_2 G_{\text{i2b}} + V_2 G_{\text{LPF}}\right) \left(G_{\text{di2}} + G_{\text{i1b}} G_{\text{v1i2}} G_{\text{di1}}\right)}{1 - G_{\text{i1b}} G_{\text{v1i2}} G_{\text{i2b}} G_{\text{v2i1}}} \tag{33}$$

$$G_p = \frac{\Delta\bar{p}_{2b}}{\Delta p_{\text{ref}}} = -\frac{T_{\text{all}}}{1 - T_{\text{all}}}. \tag{34}$$

Next, the equations for impedance are derived. Small-signal circuit models with both side LC filters are shown in Fig. 11. Z_{1bf} in Fig. 11(a) is the primary side impedance of the DAB converter including the secondary side LC filter, which can be obtained as (35) by deriving the relation for $\Delta\bar{v}_{1b}$ and $\Delta\bar{i}_{1b}$ without including the blocks related to the primary side LC filter, as shown in Fig. 12. Similarly, Z_{2bf} in Fig. 11(b) is the secondary side impedance of the DAB converter including the primary side LC filter, which can be obtained as (36) by deriving the relation for $\Delta\bar{v}_{2b}$ and $\Delta\bar{i}_{2b}$ without including the blocks related to the primary side LC filter, as shown in Fig. 13.

$$Z_{1bf} = \frac{1 + G_c G_{\text{di2}} (I_{2b} Z_{\text{LC2}} + V_{2b} G_{\text{LPF}})}{G_{\text{v1i2}} \{G_{\text{v2i1}} Z_{\text{LC2}} - G_c G_{\text{di1}} (I_{2b} Z_{\text{LC2}} + V_{2b} G_{\text{LPF}})\}} \tag{35}$$

$$Z_{2bf} = \frac{1 + G_c V_{2b} G_{\text{LPF}} (G_{\text{di2}} - G_{\text{v1i2}} Z_{\text{LC1}} G_{\text{di1}})}{G_{\text{di2}} I_{2b} G_c + G_{\text{v1i2}} Z_{\text{LC1}} (G_{\text{v2i1}} - G_{\text{di1}} I_{2b} G_c)}. \tag{36}$$

And then, primary side, and secondary side impedance Z_1 and Z_2 can be obtained as

$$Z_1 = L_1 s + r_{L1} + \frac{Z_{1bf} \left(1 + r_{C1} C_1 s\right)}{\left(r_{C1} + Z_{1bf}\right) C_1 s + 1} \tag{37}$$

$$Z_2 = L_2 s + r_{L2} + \frac{Z_{2bf} \left(1 + r_{C2} C_2 s\right)}{\left(r_{C2} + Z_{2bf}\right) C_2 s + 1}. \tag{38}$$

IV. Theory of Impedance Criterion for Bidirectional DAB Converter With Input/output LC Filters

As mentioned in Section I, the interaction between an input LC filter and a converter may cause instability, even if the converter itself is stable. This section arranges the theory of

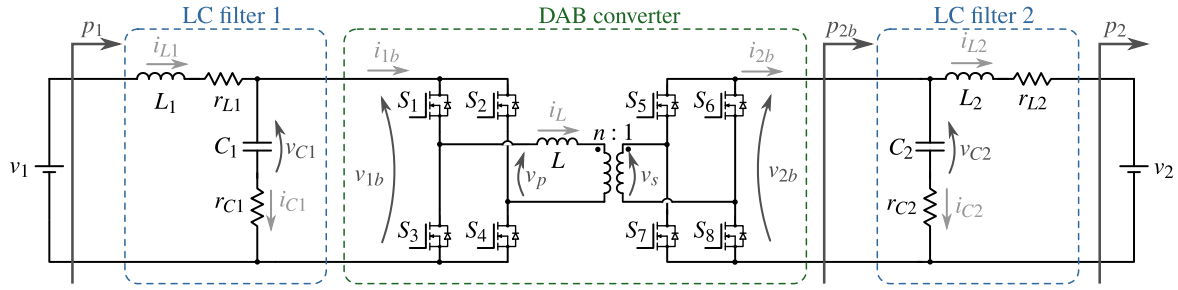

Fig. 8. Schematic of DAB converter with LC filters.

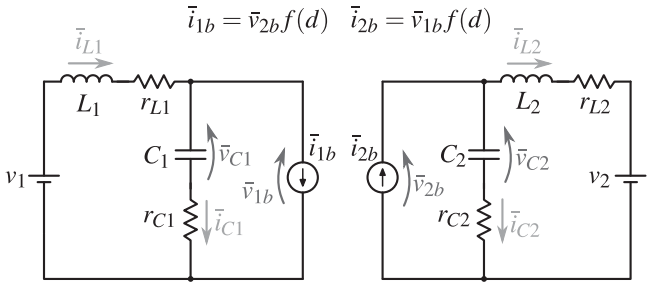

Fig. 9. Averaging model of DAB converter with LC filters.

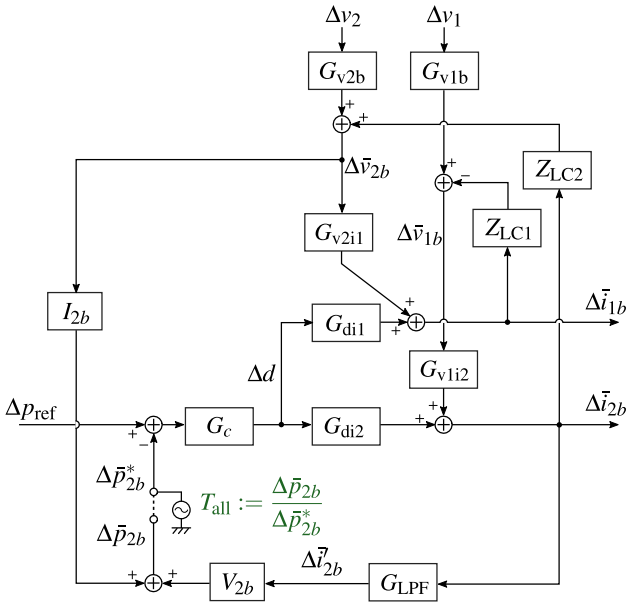

Fig. 10. Small-signal block diagram of the power-feedback system with LC filters.

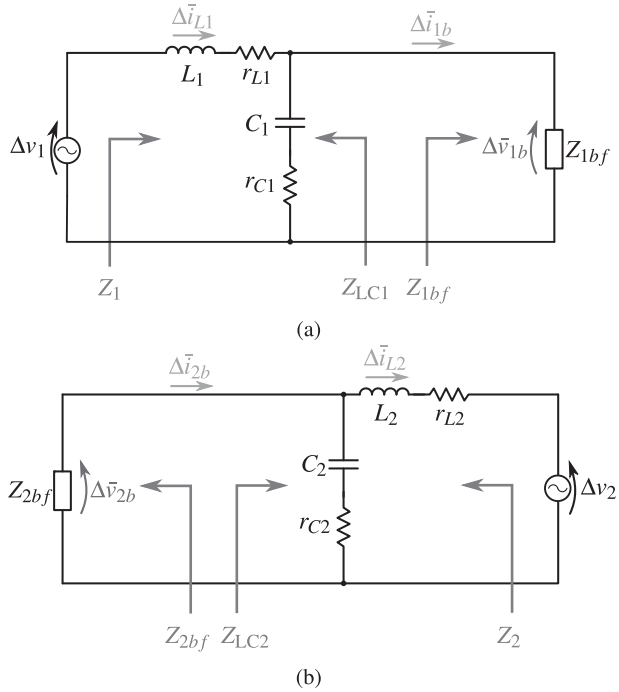

Fig. 11. Small-signal circuit models with both side LC filters. (a) Primary side. (b) Secondary side.

impedance stability criterion for the input/output LC filters and bidirectional DAB converter with power control.

Fig. 14(a) shows the primary side equivalent circuit organized by Thevenin's theorem for the primary side LC filter in Fig. 11(a), and the relationship between voltage and current from Fig. 14(a) is summarized in Fig. 14(b), where Z_{1bf} includes secondary side LC filter and Z_{1b} does not include it. From Fig. 14(b), the loop transfer functions T_{m1} and T_{m1f} can be obtained as (39) and (40). Similarly, Fig. 15(a) shows the secondary side equivalent circuit organized from Fig. 11(b), and the relationship between voltage and current from Fig. 15(a) is summarized in Fig. 15(b), where Z_{2bf} includes primary side LC filter and Z_{2b} does not include it. From Fig. 15(b), the loop transfer functions T_{m2} and T_{m2f} can be obtained as (41) and (42). If either of the loop transfer functions (39)–(42) satisfies the oscillation condition, the entire system become unstable even if the DAB converter itself is stable. In (39), for example, if $|T_{m1}| > 0$ dB when $\angle T_{m1} = 0°$, it is determined to be unstable

$$T_{m1} = -\frac{Z_{\mathrm{LC1}}}{Z_{1b}} \tag{39}$$

$$T_{m1f} = -\frac{Z_{\mathrm{LC1}}}{Z_{1bf}} \tag{40}$$

$$T_{m2} = -\frac{Z_{\mathrm{LC2}}}{Z_{2b}} \tag{41}$$

$$T_{m2f} = -\frac{Z_{\mathrm{LC2}}}{Z_{2bf}}. \tag{42}$$

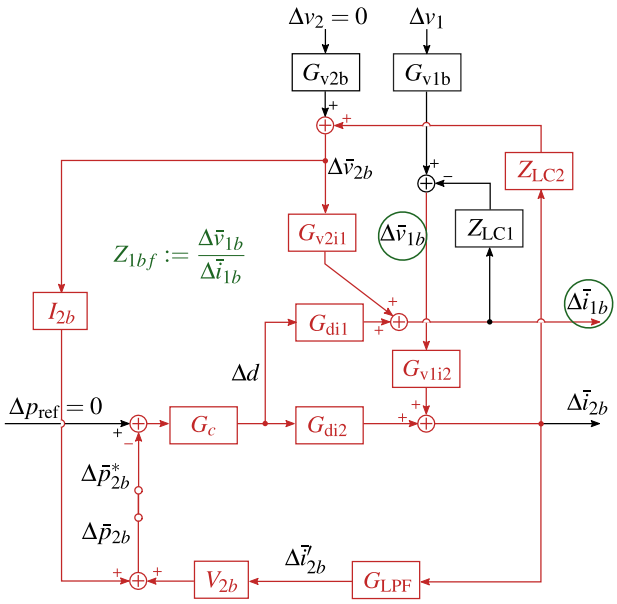

Fig. 12. Concept for deriving Z_{1bf}.

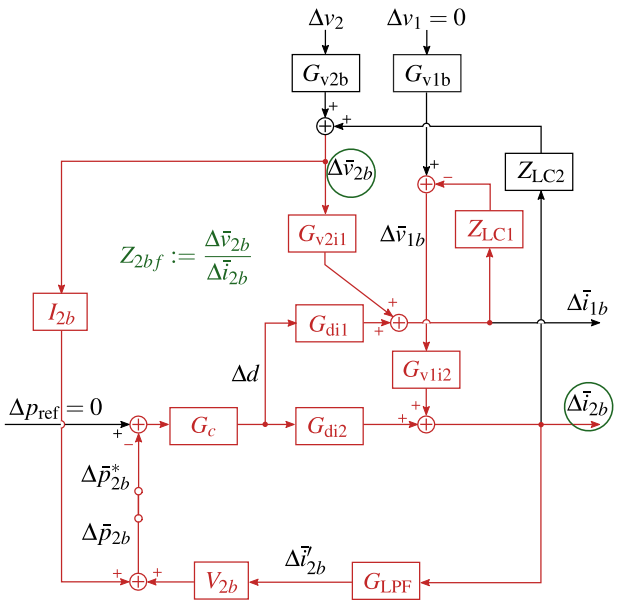

Fig. 13. Concept for deriving Z_{2bf}.

This article applies the impedance criterion by dividing the power conversion system into three subsystems, as shown in Fig. 8. At this time, each of the subsystems must be stable or passive. Therefore, this article applies the stability analysis procedure, as shown in Fig. 16, which the analysis concept is based on [50]. At first, T_{DAB} in (20) is used to ensure stability when power-feedback control is applied to the DAB converter in Fig. 1. Secondary, the stability of the LC filter connected to the primary side of the DAB converter is determined using T_{m1} in (39). Once T_{m1} is determined to be stable, combine the DAB converter and primary-side LC filter as a subsystem, and finally determine the stability when the LC filter is connected to the secondary side using T_{m2f} in (42). The stability of this entire

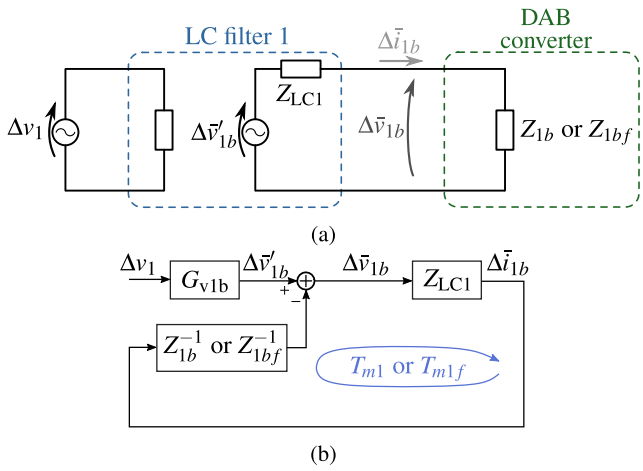

Fig. 14. Relationship of LC filter and DAB converter on primary side. (a) Equivalent circuit organized by the Thevenin's theorem. (b) Block diagram.

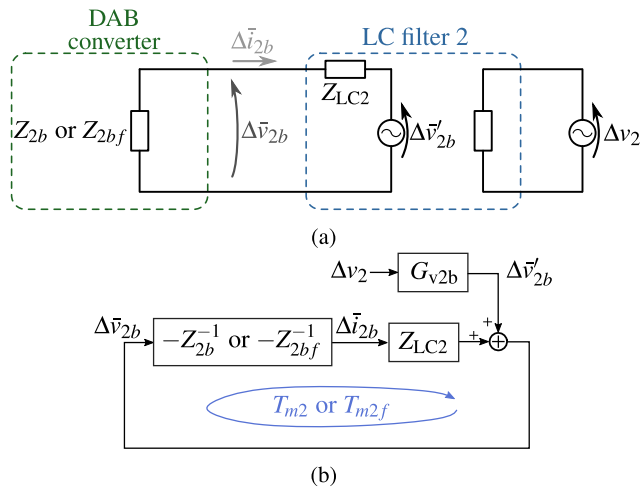

Fig. 15. Relationship of LC filter and DAB converter on secondary side. (a) Equivalent circuit organized by the Thevenin's theorem. (b) Block diagram.

system can be guaranteed if it can be determined to be stable even at T_{m2f}.

The related study [50] discusses stability analysis of multiple loops in the overall system when multiple converters are connected in parallel on a single dc bus, which the analysis is focused on total numbers of encirclements of the critical point at Nyquist diagrams. Although there is an intersection with the real axis outside the critical point on the Nyquist diagram, the system becomes stable if the total numbers of clockwise and counterclockwise encirclements of the critical point are equal to each other [49], [50], [51]. Meanwhile, this article focuses on the conventional analysis which is based on bode diagrams of the impedances in order to obtain design guidelines for the converter system clearly.

V. Experiment and Theoretical Calculation

This section performs the stability analysis discussed in Section IV using numerical calculations and confirms the system behavior through experiment. At the same time, the validity of

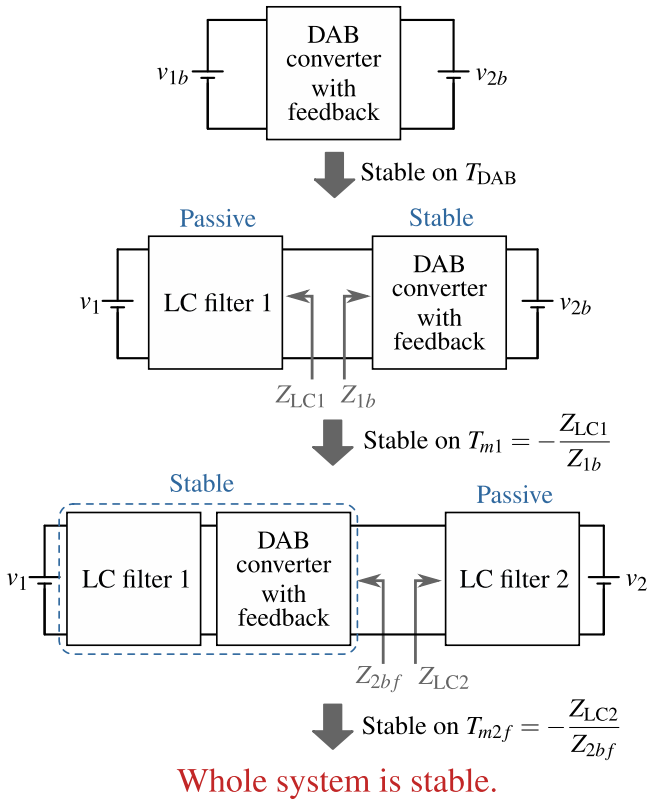

Fig. 16. Procedure of stability analysis for DAB converter in this article.

TABLE I
EXPERIMENT PARAMETERS OF DAB CONVERTER WITH FEEDBACK SYSTEM

parameters	value	parameters	value
V_1	40 V	Deadtime	197 ns
V_2	40 V	f_c	10 kHz
$n:1$	1 : 1	K_p	0.0004/W
L	45.3 μH	f_i	80 kHz
f_s	100 kHz	T_D	20 μs

TABLE II
EXPERIMENT PARAMETERS OF LC FILTER ON CASE 1

Primary side		Secondary side	
parameters	value	parameters	value
L_1	1.027 mH	L_2	1.060 mH
r_{L1}	284.3 mΩ	r_{L2}	268.3 mΩ
C_1	86.01 μF	C_2	85.68 μF
r_{C1}	415.4 mΩ	r_{C2}	432.6 mΩ
Resonant frequency	535.5 Hz	Resonant frequency	528.1 Hz
Quality factor	4.938	Quality factor	5.018

the small-signal model shown in Fig. 10 is confirmed by bode diagrams.

A structure and overview of experimental system are shown in Figs. 17 and 18. The parameters of the DAB converter and control system are shown in Table I, and the parameters of the LC filter are prepared to two cases, as shown in Tables II and III, respectively, in which Case 1 means the whole system is stable and Case 2 means the system is at the stability limit.

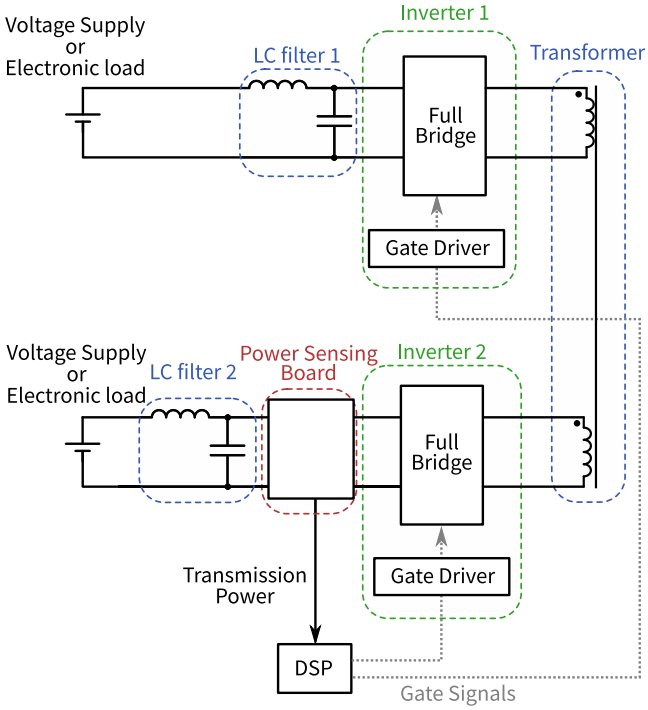

Fig. 17. Structure of experimental system.

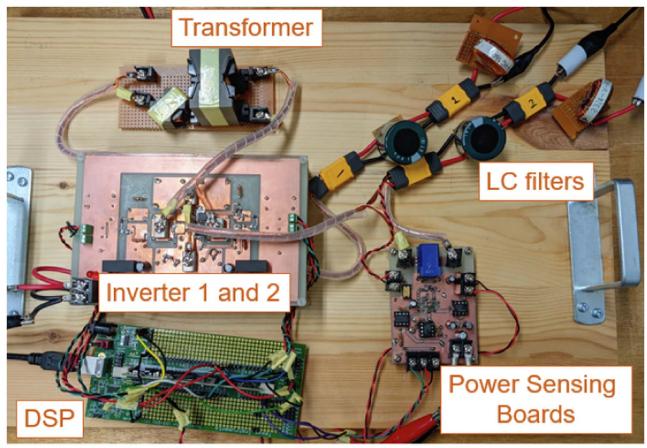

Fig. 18. Overview of experimental system.

This experimental prototype was created by dividing the circuit into small sections for each inverter boards, transformer, power sensing board, and LC filters. MOSFETS "BSC093N15NS5" from Infineon were used as the switching device and bootstrap drive circuits were implemented using an isolated gate driver IC "ADUM4224" from Analog Devices on the inverter boards. The transformer was made by using "PC47 PQ40-40" ferrite cores from TDK, and the series inductance L was set by adding a inductor using "PC40 RM10Z-12" from TDK in series with the primary side of the transformer. In the power sensing board, the secondary side voltage v_{2b} and current i_{2b} were detected as analog voltage signals, and the voltage signal about the transmission power p_{2b} was obtained using analog multiplier "AD633" from Analog Devices. The voltage

TABLE III
EXPERIMENT PARAMETERS OF LC FILTER ON CASE 2

Primary side parameters	value	Secondary side parameters	value
L_1	1.027 mH	L_2	1.060 mH
r_{L1}	284.3 mΩ	r_{L2}	268.3 mΩ
C_1	9.724 μF	C_2	9.574 μF
r_{C1}	1.283 Ω	r_{C2}	1.401 Ω
Resonant frequency	1.593 kHz	Resonant frequency	1.580 kHz
Quality factor	6.557	Quality factor	6.303

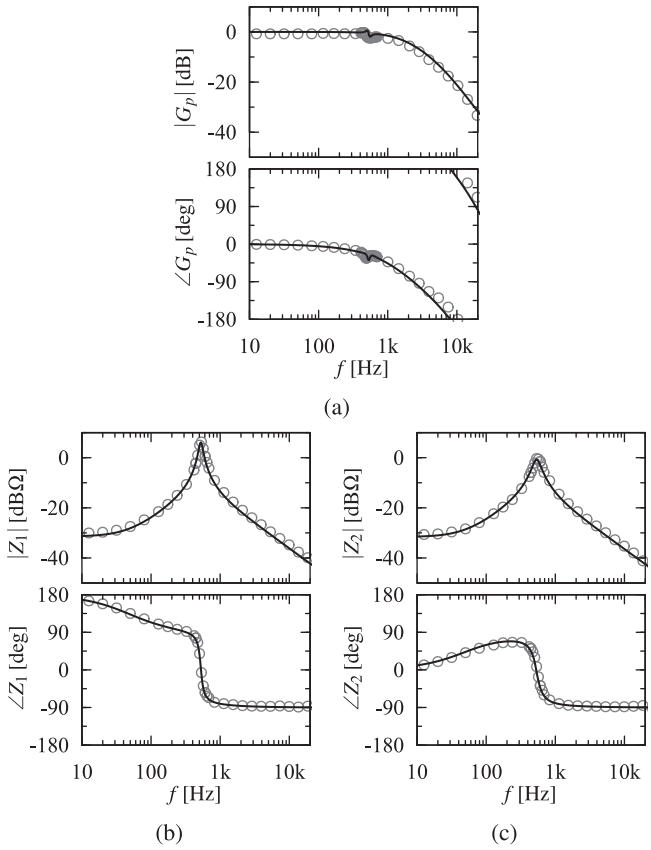

Fig. 19. Bode diagrams of the small-signal characteristics, lines represent theoretical calculation, and markers represents experimental results at $D = 0.4$, (a) G_p. (b) Z_1 with additional 0.1 Ω resistor in series to L_1. (c) Z_2 with additional 0.1 Ω resistor in series to L_2.

signal of p_{2b} was sent to the analog-to-digital conversion (ADC) terminal of the digital signal processor (DSP) "TMS320F28335" from Texas Instruments. The gate signals to each switching device was generated from the feedback calculation in the DSP, including the deadtime, and the gate signals were input to the gate driver IC on the inverter boards.

A. Validation of Small-Signal Characteristics

Under the parameters in Tables I and II and $D = 0.4$, the validity of the small-signal model of Fig. 10 derived in this article will be confirmed by experiment. The obtained bode diagram is shown in Fig. 19, where the black lines represent the theoretical calculations of (34), (37), and (38), and the markers represent

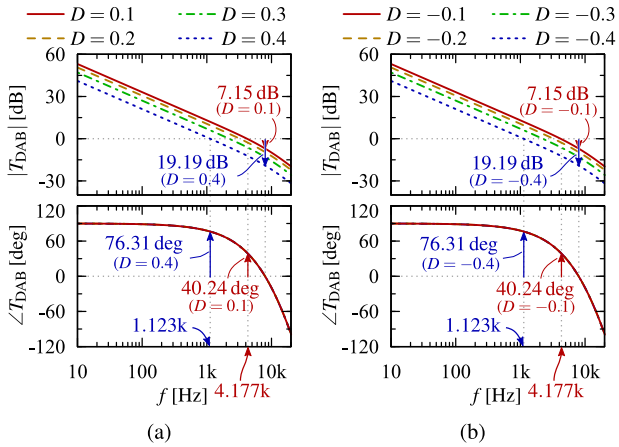

Fig. 20. Bode diagrams of T_{DAB} without LC filters obtained by theoretical calculation. (a) $D > 0$. (b) $D < 0$.

the experimental measurement results. In both cases, the characteristics of the theoretical calculations and the experimental results generally matched, which confirms the validity of the analysis in this article.

For the measurement, the DSP debugging function was used to adjust P_{ref} to set the steady-state operating point $D = 0.4$ before injecting a small-signal fluctuation. The bode diagram of the closed-loop transfer function G_p [Fig. 19(a)] was measured by injecting a small-signal voltage into the ADC terminals of the DSP to internally inject a small-signal fluctuation Δp_{ref} into p_{ref} and observing the variation in the detection signal voltage of p_{2b} that is feedback from the power sensing board to the other ADC inputs. At that time, the conversion gain from the input voltage of the ADC terminals to the digital value inside the DSP was set to be adjusted by Δp_{ref} and Δp_{2b}. The bode diagram of Z_1 Fig. 19(b) was measured by injecting a small-signal fluctuation Δv_1 to the primary side voltage v_1 and observing a small-signal variation of primary side inductor current Δi_{L1}. At that time, a noninductive resistor 0.1 Ω for current detection is connected in series to the inductor L_1 on the experimental prototype, and in the numerical calculation of Z_1, the equivalent series resistance r_{L1} was set to $r_{L1} = 284.3 + 100\,\mathrm{m\Omega}$. The bode diagram of Z_2 [Fig. 19(c)] was also measured by connecting a noninductive resistor 0.1 Ω for current detection in series to the inductor L_2, and applying a small-signal fluctuation Δv_2 to the secondary side voltage v_2 and observing a small-signal fluctuation Δi_{L2} of the secondary side inductor current.

B. Stability Analysis of the DAB Converter With Input/output LC Filters

Bode diagrams of T_{DAB} at specific parameters in Table I are shown in Fig. 20, where $V_{1b} = V_1 = 40\,\mathrm{V}, V_{2b} = V_2 = 40\,\mathrm{V}$. From Fig. 20, it can be seen that the characteristics of T_{DAB} depend on $|D|$, regardless of the sign of D, and the DAB converter with power-feedback control is stable in the range of $|D| = 0.1$ to 0.4 under the parameters in Table I.

After T_{DAB} was determined to be stable, the stability of T_{m1}, T_{m2f} was confirmed under the parameters of Case 1

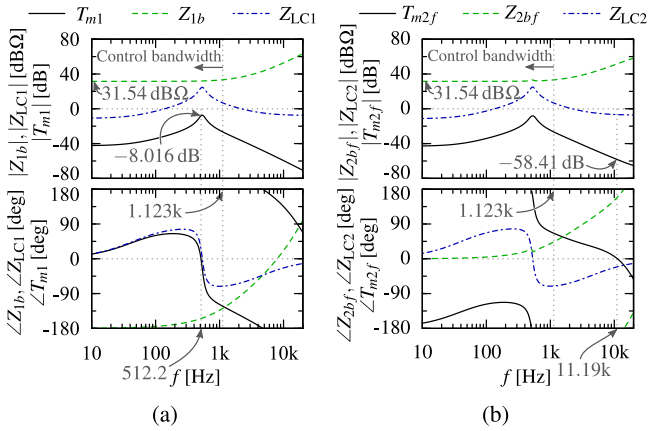

Fig. 21. Bode diagrams for impedance criterion on Case 1 at $D = 0.4$. (a) Primary side. (b) Secondary side.

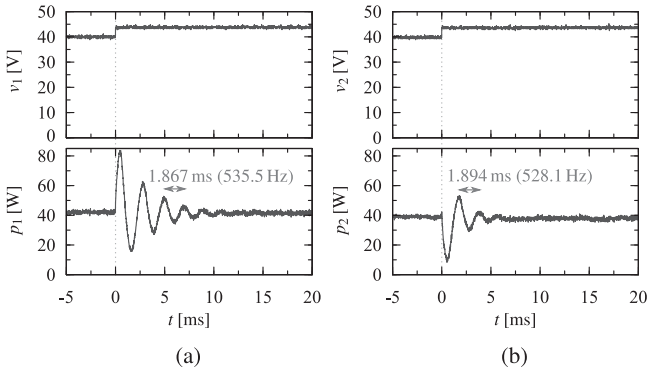

Fig. 22. Experimental measurement of converter's transient response on Case 1 at $D = 0.4$. (a) Primary side with step variation of $+4$ V for v_1. (b) Secondary side with step variation of $+4$ V for v_2.

(Table II). Fig. 21 shows the bode diagram of T_{m1}, T_{m2f} in Case 1 by numerical calculation, where $D = 0.4$: the converter transfers power from primary to secondary. The gain margin of T_{m1} in Fig. 21(a) was 8.016 dB and that of T_{m2f} in Fig. 21(b) was 58.41 dB, which confirms that the entire system including the LC filter was determined as stable. Under Case 1 and $D = 0.4$, the experimental measurement of the converter's voltage step response is shown in Fig. 22, which the voltage variation in the dc bus is mainly caused by load variations within the connected power grid. Fig. 22(a) shows the response of p_1 when a step variation of $+4$ V was applied to the primary side voltage v_1, and Fig. 22(b) shows the response of p_2 when a step variation of $+4$ V was applied to the secondary side voltage v_2. Although ringing due to resonance occurred in both cases, p_1 and p_2 converged to certain values by power-feedback control, and it was confirmed that the system was stable, as determined by T_{m1}, T_{m2f}. Similarly, for the reverse transmission ($D = -0.4$) in Case 1, the gain margin of T_{m1} was 47.96 dB in Fig. 23(a) and that of T_{m2f} was 7.032 dB in Fig. 23(b), which indicates that the system was stable. The transient response by voltage step variations in reverse transmission (24) confirmed that the system was stable. Also, Fig. 22 confirms that the oscillation of p_1 was more severe than that of the secondary side, and Fig. 24

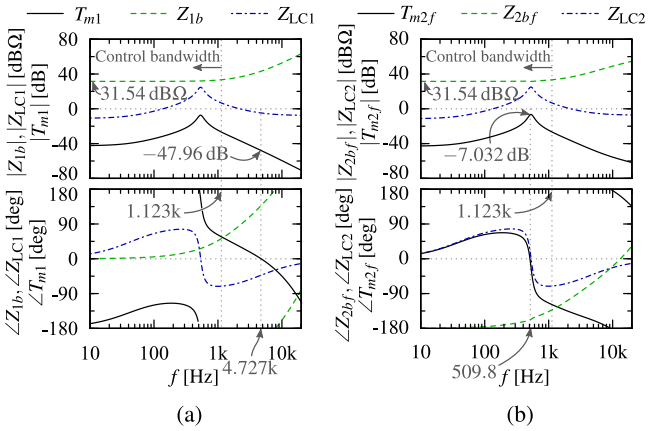

Fig. 23. Bode diagrams for impedance criterion on case 1 at $D = -0.4$. (a) Primary side. (b) Secondary side.

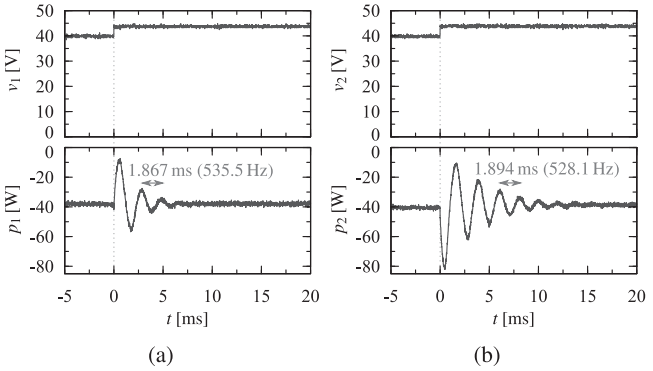

Fig. 24. Experimental measurement of converter's transient response on case 1 at $D = -0.4$. (a) Primary side with step variation of $+4$ V for v_1. (b) Secondary side with step variation of $+4$ V for v_2.

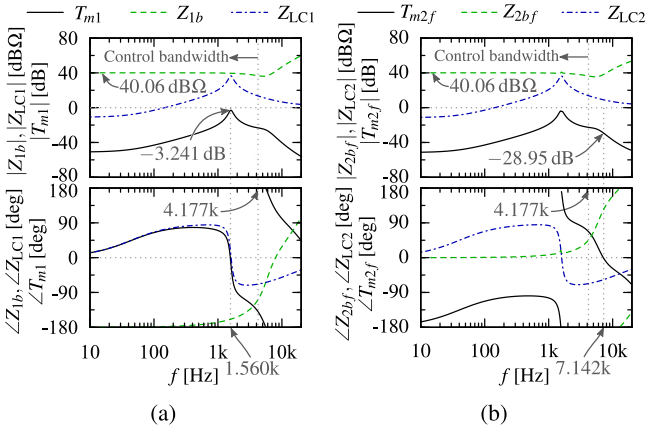

Fig. 25. Bode diagrams for impedance criterion on Case 2 at $D = 0.1$. (a) Primary side. (b) Secondary side.

confirms that the oscillation of p_2 was more severe than that of the primary side.

Next, under the condition that T_{DAB} was stable, the stability of T_{m1}, T_{m2f} was confirmed under Case 2 (Table III). Fig. 25 shows the bode diagrams of T_{m1}, T_{m2f} in Case 2 obtained by numerical calculations, where $D = 0.1$. From Fig. 25(a), the gain margin of T_{m1} was as small as 3.241 dB, which indicates

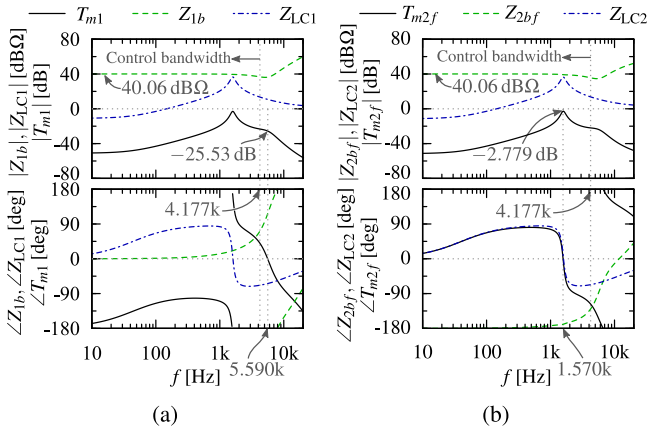

Fig. 26. Bode diagrams for impedance criterion on Case 2 at $D = -0.1$. (a) Primary side. (b) Secondary side.

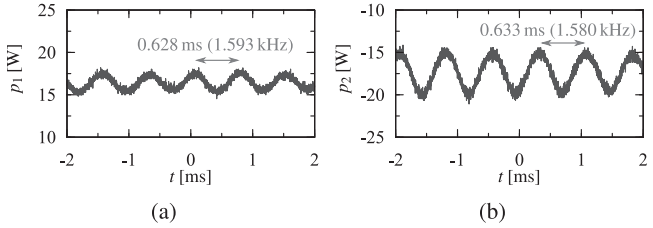

Fig. 27. Experimental measurement of converter's steady-state behavior on Case 2. (a) Primary side at $D = 0.1$. (b) Secondary side at $D = -0.1$.

that the system was close to the stability limit. For Case 2 with reverse transmission ($D = -0.1$), the gain margin of T_{m1} was 25.53 dB from Fig. 26(a), but the gain margin of T_{m2f} was as small as 2.779 dB from Fig. 26(b), which indicates that the system was also close to the stability limit as in $D = 0.1$. The system's transient behavior at this time is shown in Fig. 27, with the power waveform oscillation at the resonant frequency in the steady state.

VI. Discussion

It is necessary to consider the operating range of the steady-state phase shift ratio D when designing the power stage and control system of DAB converter. As described in Sections III-A and V-B, the stability and responsiveness of the DAB converter with power-feedback control varies with the steady-state value of the phase shift ratio D, and the responsiveness of the control system decreases as $|D|$ increases. In particular, the responsiveness of the system decreases around $|D| = 0.5$, which is the maximum operation value. The relationship between d and the transmission power $\bar{p}$ is described by (3), which means that the maximum value of the power is determined by the parameters of the power stage shown in Fig. 1. Therefore, the neighborhood of the operating point $|D| = 0.5$ should be avoided in designing the DAB converter by estimate the maximum transmission power excessively. In contrast, it should be mentioned that the plant system gain will increase when $|D|$ is close to 0, as shown in Fig. 20, which means that instability may occur in the DAB converter with control system at light loads, as described in [48]. Therefore, it is necessary to design the controller G_c so as to ensure stability and responsiveness within an assumed range of the operating point D.

In addition, it is important how to isolate the whole system to some subsystems for impedance stability criterion when LC filters are connected on both sides. As described in [35], this method requires that each of the two subsystems should be stable individually, and if the subsystems themselves are unstable, this analysis method cannot be applied. The bidirectional system treated in this article should ensure stability by combining LC filters and DAB converters one by one, as shown in Fig. 16. Since the converter performs bidirectional transmission, the input and output sides are interchanged depending on the direction of power transmission. Within the power control bandwidth, the DAB converter from the input side behaves as a CPL, and the interaction between the LC filter on the input side and the converter may cause instability, which trend was seen in Figs. 22 and 24. As summarized in [43], the impedance gain of the converter itself in the control bandwidth can be approximated as the small signal impedance of the CPL [53]. In this article, the impedance gains $|Z_{1b}|$, $|Z_{1bf}|$, $|Z_{2b}|$, and $|Z_{2bf}|$ can be approximated as (43) and (44) in the control bandwidth based on [53]. For example, this article assumes $V_1 = V_2 = 40\,\mathrm{V}$ and since $D = \pm 0.4$ in Case 1, $|P_1| = |P_2| = 42.38\,\mathrm{W}$ can be obtained from (3) under no conversion loss. Therefore, from (43) and (44), $|Z_{1b}| = |Z_{1bf}| = |Z_{2b}| = |Z_{2bf}| = 31.54\,\mathrm{dB\Omega}$ can be obtained, which is consistent with the calculation results within the control bandwidth shown in Figs. 21 and 23. Similarly, since $D = \pm 0.1$ in Case 2, $|P_1| = |P_2| = 15.89\,\mathrm{W}$ can be obtained from (3). Therefore, from (43) and (44), $|Z_{1b}| = |Z_{1bf}| = |Z_{2b}| = |Z_{2bf}| = 40.06\,\mathrm{dB\Omega}$ can be obtained, which is consistent with the calculation results within the control bandwidth shown in Figs. 25 and 26. Of course, the control bandwidth will be limited up to $1/10$ of switching frequency

$$|Z_{1b}| \sim \frac{V_1^2}{|P_1|}, |Z_{1bf}| \sim \frac{V_1^2}{|P_1|} \tag{43}$$

$$|Z_{2b}| \sim \frac{V_2^2}{|P_2|}, |Z_{2bf}| \sim \frac{V_2^2}{|P_2|}. \tag{44}$$

If the peak gain at the resonance point of the LC filter impedance Z_{LC1}, Z_{LC2} is sufficiently smaller than that of converter itself shown in (43) and (44), then the system becomes stable. The peak impedance gain of the primary side LC filter at the resonance point, $|Z_{LC1r}|$, can be obtained as (45) by setting $s = j\omega = j/\sqrt{L_1 C_1}$. Similarly, the peak impedance gain of the secondary side LC filter $|Z_{LC2r}|$, can be obtained as (46)

$$|Z_{LC1r}| = \frac{\sqrt{(C_1 r_{C1} r_{L1} + L_1)^2 + C_1 L_1 (r_{C1} - r_{L1})^2}}{C_1 (r_{L1} + r_{C1})} \tag{45}$$

$$|Z_{LC2r}| = \frac{\sqrt{(C_2 r_{C2} r_{L2} + L_2)^2 + C_2 L_2 (r_{C2} - r_{L2})^2}}{C_2 (r_{L2} + r_{C2})}. \tag{46}$$

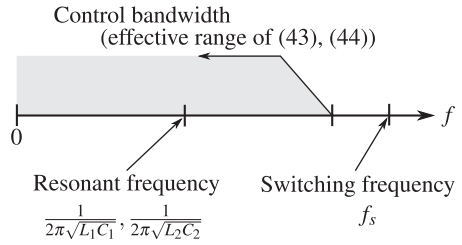

Fig. 28. Relationships of the frequency-domain assumptions for the simplified design in this article.

Therefore, it can be said that system stability will be sufficiently guaranteed if the input/output LC filter is designed to satisfy the conditions (47), where $P_{1\max}$ and $P_{2\max}$ are maximum transmission power of the system at primary and secondary side designed by users. Also, the resonance frequency of the LC filter should be set within the control bandwidth so that ringing in the transient response may be suppressed. The frequency-domain assumptions for this simplified design can be summarized, as in Fig. 28

$$|Z_{LC1r}| < \frac{V_1^2}{|P_{1\max}|}, |Z_{LC2r}| < \frac{V_2^2}{|P_{2\max}|}. \tag{47}$$

It should be noted that the above equations are theoretical conditions for stable design, and the parameters in Tables II and III used in this stability analysis are only actual measured values. In practical design, errors in circuit parameters should also be taken into account. The parameters of capacitors and inductors used in LC filters may deviate from nominal values up to $\pm 20\%$, which can significantly affect the results of stability analysis. In particular, the peak gain of the LC filters (45) and (46) increases as L_1, L_2 increases and C_1, C_2 decreases, and the system tends to be more unstable. For example, let $L_1 \to 1.2L_1$ (L_1 increases by 20%) and $C_1 \to 0.8C_1$ (C_1 decreases by 20%), then $|Z_{LC1r}|$ was changed as (48). Similarly, let $L_2 \to 1.2L_2$ (L_2 increases by 20%) and $C_2 \to 0.8C_2$ (C_2 decreases by 20%), then $|Z_{LC2r}|$ was changed as (49), which confirms that the peak gain was increased compared to (45) and (46). Hence, by using (48) and (49), the condition (47) becomes more strict, and practical design with consideration of parameter errors may be possible.

$$|Z_{LC1r}| = \frac{\sqrt{(C_1 r_{C1} r_{L1} + 1.5L_1)^2 + 1.5C_1L_1(r_{C1} - r_{L1})^2}}{C_1(r_{L1} + r_{C1})} \tag{48}$$

$$|Z_{LC2r}| = \frac{\sqrt{(C_2 r_{C2} r_{L2} + 1.5L_2)^2 + 1.5C_2L_2(r_{C2} - r_{L2})^2}}{C_2(r_{L2} + r_{C2})}. \tag{49}$$

Although this article discusses stability analysis and design guidelines when LC filters are connected on both sides of the converter, this discussion can be applied to the case where LC filters are connected on only one side. For example, if only the primary LC filter is connected, the analysis method can be performed by T_{m1} in Fig. 16, and the same discussion can be given for the design guideline in this section by setting $L_2 = 0\,\mathrm{H}, r_{L2} = 0\,\Omega$ in (46).

The modeling methods, stability analysis, and system design guidelines discussed in this article can be extended to triple phase shift (TPS), a more general modulation scheme than SPS which is applied in this article. TPS is a modulation method for DAB converter that performs phase shift operation not only between inverters but also between legs inside the inverters, and its optimal operation enables higher efficiency power conversion than SPS [10], [30]. Other typical DAB converter modulation methods include extended phase shift (EPS) and dual phase shift (DPS). SPS, EPS, and DPS can be considered as special cases of TPS [9]. The averaging model of the DAB converter operating with TPS modulation can be represented as a current sources depending on the phase shift ratios and input/output voltage [27], which is equivalent to the circuit model configuration shown in Fig. 4. Therefore, the stability analysis method and system design guideline treated in this article can be applied not only to SPS but also EPS, DPS, and TPS.

Finally, it can be summarized about the DAB converter design procedure with SPS modulation as follows.

1) The neighborhood of the maximum operating point $|D| = 0.5$ should be avoided in designing the power stage of DAB converter itself.
2) The feedback controller G_c should be designed to ensure stability and responsiveness based on (20), while sweeping D within the expected range.
3) Input/output LC filters should be designed to satisfy the conditions (47) and Fig. 28.
4) Stability of the whole power conversion system should be guaranteed based on the procedure summarized in Fig. 16.

VII. Conclusion

This article considers the dynamic model of bidirectional DAB converter with power-feedback control which input and output LC filters were connected. Experimental results confirmed the validity of the dynamic model considered in this article. In addition, the procedure of impedance stability criterion and practical design guidelines were discussed for the bidirectional DAB converter. It should be mentioned that the analysis target should be separate to "stable" subsystem and apply the impedance criterion by combining LC filters and DAB converters one by one. Experimental results also confirmed that the stability analysis results in this article matched to the behavior of the prototype system.

Appendix

Equation (13) is derived in this Appendix. Since $|d| = d$ with $d \geq 0$, (4) becomes (50), and (51) can be obtained by differentiating (50) about d

$$f(d) = \frac{n}{\omega_s L}\pi d(1-d) \tag{50}$$

$$f'(d) = \frac{n}{\omega_s L}\pi(1-2\,d). \tag{51}$$

Similarly, (53) can be obtained through (52) since $|d| = -d$ with $d < 0$

$$f(d) = \frac{n}{\omega_s L}\pi d(1+d) \tag{52}$$

$$f'(d) = \frac{n}{\omega_s L}\pi(1+2\,d). \tag{53}$$

By combining (51) and (53), $f'(d)$ can be obtained for all d.

$$f'(d) = \frac{n}{\omega_s L}\pi(1 - 2|d|). \tag{54}$$

Finally, (13) can be obtained by considering $d = D$.

REFERENCES

[1] A. Jäger-Waldau, "Snapshot of photovoltaics—February 2020," *Energies*, vol. 13, no. 4, Feb. 2020, Art. no. 930.

[2] J. J. Justo, F. Mwasilu, J. Lee, and J.-W. Jung, "AC-microgrids versus DC-microgrids with distributed energy resources: A review," *Renew. Sustain. Energy Rev.*, vol. 24, pp. 387–405, Aug. 2013.

[3] L. Meng et al., "Review on control of DC microgrids and multiple microgrid clusters," *IEEE J. Emerg. Sel. Topics Power Electron.*, vol. 5, no. 3, pp. 928–948, Sep. 2017.

[4] M. Forouzesh, Y. P. Siwakoti, S. A. Gorji, F. Blaabjerg, and B. Lehman, "Step-up DC–DC converters: A comprehensive review of voltage-boosting techniques, topologies, and applications," *IEEE Trans. Power Electron.*, vol. 32, no. 12, pp. 9143–9178, Dec. 2017.

[5] Y. Imamura, H. A. Ramadan, S. Yang, G. M. Dousoky, and M. Shoyama, "Seamless dynamic model for DC–DC converters applicable to bi-directional power transfer," in *Proc. IEEE 15th Eur. Conf. Power Electron. Appl.*, 2013, pp. 1–10.

[6] R. W. A. A. De Doncker, D. M. Divan, and M. H. Kheraluwala, "A three-phase soft-switched high-power-density DC/DC converter for high-power applications," *IEEE Trans. Ind. Appl.*, vol. 27, no. 1, pp. 63–73, Jan./Feb. 1991.

[7] M. N. Kheraluwala, R. W. Gascoigne, D. M. Divan, and E. D. Baumann, "Performance characterization of a high-power dual active bridge DC-to-DC converter," *IEEE Trans. Ind. Appl.*, vol. 28, no. 6, pp. 1294–1301, Nov./Dec. 1992.

[8] S. Inoue and H. Akagi, "A bidirectional isolated DC–DC converter as a core circuit of the next-generation medium-voltage power conversion system," *IEEE Trans. Power Electron.*, vol. 22, no. 2, pp. 535–542, Mar. 2007.

[9] B. Zhao, Q. Song, W. Liu, and Y. Sun, "Overview of dual-active-bridge isolated bidirectional DC-DC converter for high-frequency-link power-conversion system," *IEEE Trans. Power Electron.*, vol. 29, no. 8, pp. 4091–4106, Aug. 2014.

[10] J. Huang, Y. Wang, Z. Li, and W. Lei, "Unified triple-phase-shift control to minimize current stress and achieve full soft-switching of isolated bidirectional DC–DC converter," *IEEE Trans. Ind. Electron.*, vol. 63, no. 7, pp. 4169–4179, Jul. 2016.

[11] I. Tank and S. Mali, "Renewable based DC microgrid with energy management system," in *Proc. IEEE Int. Conf. Signal Process. Inf. Commun. Energy Syst.*, 2015, pp. 1–5.

[12] A. C. Luna et al., "Mixed-integer-linear-programming-based energy management system for hybrid PV-wind-battery microgrids: Modeling, design, and experimental verification," *IEEE Trans. Power Electron.*, vol. 32, no. 4, pp. 2769–2783, Apr. 2017.

[13] S. Shao et al., "Modeling and advanced control of dual-active-bridge DC–DC converters: A review," *IEEE Trans. Power Electron.*, vol. 37, no. 2, pp. 1524–1547, Feb. 2022.

[14] H. Qin and J. W. Kimball, "Closed-loop control of DC–DC dual-active-bridge converters driving single-phase inverters," *IEEE Trans. Power Electron.*, vol. 29, no. 2, pp. 1006–1017, Feb. 2014.

[15] D. Segaran, D. G. Holmes, and B. P. McGrath, "Enhanced load step response for a bidirectional DC–DC converter," *IEEE Trans. Power Electron.*, vol. 28, no. 1, pp. 371–379, Jan. 2013.

[16] W. Song, N. Hou, and M. Wu, "Virtual direct power control scheme of dual active bridge DC–DC converters for fast dynamic response," *IEEE Trans. Power Electron.*, vol. 33, no. 2, pp. 1750–1759, Feb. 2018.

[17] C. Chang, Y. Xu, B. Bian, and X. Zhao, "A high-precision CV/CC AC–DC converter based on cable and inductance compensation schemes," *IEEE Trans. Power Electron.*, vol. 31, no. 9, pp. 6372–6382, Sep. 2016.

[18] N. Tashakor, E. Farjah, and T. Ghanbari, "A bidirectional battery charger with modular integrated charge equalization circuit," *IEEE Trans. Power Electron.*, vol. 32, no. 3, pp. 2133–2145, Mar. 2017.

[19] J. Rojas et al., "Partial power DC-DC converter for electric vehicle fast charging stations," in *Proc. IEEE 43rd Annu. Conf. Ind. Electron. Soc.*, 2017, pp. 5274–5279.

[20] A. Rachid, H. E. Fadil, and F. Giri, "Dual stage CC-CV charge method for controlling DC-DC power converter in BEV charger," in *Proc. IEEE 19th Mediterranean Electrotechnical Conf.*, 2018, pp. 74–79.

[21] A. R. Rodríguez Alonso, J. Sebastian, D. G. Lamar, M. M. Hernando, and A. Vazquez, "An overall study of a dual active bridge for bidirectional DC/DC conversion," in *Proc. IEEE Energy Convers. Congr. Expo.*, Atlanta, GA, USA, 2010, pp. 1129–1135.

[22] H. Bai et al., "The dynamic model and hybrid phase-shift control of a dual-active-bridge converter," in *Proc. IEEE 34th Annu. Conf. Ind. Electron.*, Orlando, FL, 2008, pp. 2840–2845.

[23] H. Qin and J. W. Kimball, "Generalized average modeling of dual active bridge DC–DC converter," *IEEE Trans. Power Electron.*, vol. 27, no. 4, pp. 2078–2084, Apr. 2012.

[24] V. M. Iyer, S. Gulur, and S. Bhattacharya, "Hybrid control strategy to extend the ZVS range of a dual active bridge converter," in *Proc. IEEE Appl. Power Electron. Conf. Expo.*, 2017, pp. 2035–2042.

[25] A. Pal, S. Kapat, K. Jha, and A. Tiwari, "Discrete-time framework for digital control design in a high-frequency dual active bridge converter," in *Proc. IEEE Appl. Power Electron. Conf. Expo.*, San Antonio, TX, 2018, pp. 2264–2270.

[26] J. A. Mueller and J. W. Kimball, "An improved generalized average model of DC–DC dual active bridge converters," *IEEE Trans. Power Electron.*, vol. 33, no. 11, pp. 9975–9988, Nov. 2018.

[27] S. S. Shah and S. Bhattacharya, "A simple unified model for generic operation of dual active bridge converter," *IEEE Trans. Ind. Electron.*, vol. 66, no. 5, pp. 3486–3495, May 2019.

[28] K. Zhang, Z. Shan, and J. Jatskevich, "Large- and small-signal average-value modeling of dual-active-bridge DC–DC converter considering power losses," *IEEE Trans. Power Electron.*, vol. 32, no. 3, pp. 1964–1974, Mar. 2017.

[29] P. Wang, X. Chen, C. Tong, P. Jia, and C. Wen, "Large- and small-signal average-value modeling of dual-active-bridge DC–DC converter with triple-phase-shift control," *IEEE Trans. Power Electron.*, vol. 36, no. 8, pp. 9237–9250, Aug. 2021.

[30] B. Liu, P. Davari, and F. Blaabjerg, "An optimized control scheme to reduce the backflow power and peak current in dual active bridge converters," in *Proc. IEEE Appl. Power Electron. Conf. Expo.*, Anaheim, CA, USA, 2019, pp. 1622–1628.

[31] L. James et al., "A fast direct power digital control strategy for dual active bridge DC–DC converters," in *Proc. IEEE Int. Power Electron. Conf.*, 2022, pp. 1850–1857.

[32] H. Wang et al., "A stabilization method of LC input filter in DC microgrids feeding constant power loads," in *Proc. IEEE Energy Convers. Congr. Expo.*, 2017, pp. 4433–4438.

[33] Y. Guan, Y. Xie, Y. Wang, Y. Liang, and X. Wang, "An active damping strategy for input impedance of bidirectional dual active bridge DC–DC converter: Modeling, shaping, design, and experiment," *IEEE Trans. Ind. Electron.*, vol. 68, no. 2, pp. 1263–1274, Feb. 2021.

[34] R. D. Middlebrook, "Input filter considerations in design and application of switching regulators," in *Proc. IEEE Conf. Rec. IAS Annu. Meeting*, 1976, pp. 366–382.

[35] C. M. Wildrick et al., "A method of defining the load impedance specification for a stable distributed power system," *IEEE Trans. Power Electron.*, vol. 10, no. 3, pp. 280–285, May 1995.

[36] P. Huynh and B. H. Cho, "A new methodology for the stability analysis of large-scale power electronics systems," *IEEE Trans. Circuits Syst. I: Fundam. Theory Appl.*, vol. 45, no. 4, pp. 377–385, Apr. 1998.

[37] S. D. Sudhoff, S. F. Glover, P. T. Lamm, D. H. Schmucker, and D. E. Delisle, "Admittance space stability analysis of power electronic systems," *IEEE Trans. Aerosp. Electron. Syst.*, vol. 36, no. 3, pp. 965–973, Jul. 2000.

[38] T. Suntio, I. Gadoura, and K. Zenger, "Input filter interactions in peak-current-mode-controlled buck converter operating in CICM," *IEEE Trans. Ind. Electron.*, vol. 49, no. 1, pp. 76–86, Feb. 2002.

[39] X. Feng, J. Liu, and F. C. Lee, "Impedance specifications for stable DC distributed power systems," *IEEE Trans. Power Electron.*, vol. 17, no. 2, pp. 157–162, Mar. 2002.

[40] X. Wang, R. Yao, and F. Rao, "Three-step impedance criterion for small-signal stability analysis in two-stage DC distributed power systems," *IEEE Power Electron. Lett.*, vol. 1, no. 3, pp. 83–87, Sep. 2003.

[41] S. Abe, M. Hirokawa, M. Shoyama, and T. Ninomiya, "Optimal bus capacitance design for system stability in on-board distributed power architecture," in *Proc. IEEE 13th Int. Power Electron. Motion Control Conf.*, 2008, pp. 393–399.

[42] M. Cespedes, L. Xing, and J. Sun, "Constant-power load system stabilization by passive damping," *IEEE Trans. Power Electron.*, vol. 26, no. 7, pp. 1832–1836, Jul. 2011.

[43] X. Zhang, X. Ruan, H. Kim, and C. K. Tse, "Adaptive active capacitor converter for improving stability of cascaded DC power supply system," *IEEE Trans. Power Electron.*, vol. 28, no. 4, pp. 1807–1816, Apr. 2013.

[44] X. Zhang, Q. -C. Zhong, and W. -L. Ming, "A virtual RLC damper to stabilize DC/DC converters having an LC input filter while improving the filter performance," *IEEE Trans. Power Electron.*, vol. 31, no. 12, pp. 8017–8023, Dec. 2016.
[45] F. Feng, X. Zhang, F. Lin, and H. B. Gooi, "Impedance modeling and stability analysis of dual active bridge converter with LC input filter," *CES Trans. Elect. Mach. Syst.*, vol. 2, no. 3, pp. 289–295, Sep. 2018.
[46] F. Lin, X. Zhang, and F. Feng, "Modeling and stability analysis of the cascaded dual active bridge converter system with considerations of the controller parameters," in *Proc. IEEE 10th Int. Conf. Power Electron. ECCE Asia*, 2019, pp. 1817–1820.
[47] S. Cyriac, B. Haritha, T. Kobaku, and R. Ramchand, "Virtual impedance-based stabilization of dual active bridge converter cascaded with LC filter," in *Proc. IEEE Int. Conf. Power Electron. Drives Energy Syst.*, 2020, pp. 1–6.
[48] Y. Sun, S. Yan, G. Xu, G. Deng, and M. Su, "Stability analysis of dual active bridge converter with input filter and constant power load," *IEEE J. Emerg. Sel. Topics Ind. Electron.*, vol. 3, no. 3, pp. 658–669, Jul. 2022.
[49] M. Vidyasagar, R. K. Bertschmann, and C. S. Sallaberger, "Some simplifications of the graphical Nyquist criterion," *IEEE Trans. Autom. Control*, vol. 33, no. 3, pp. 301–305, Mar. 1988.
[50] X. Wang, F. Blaabjerg, and P. C. Loh, "An impedance-based stability analysis method for paralleled voltage source converters," in *Proc. IEEE Int. Power Electron. Conf.*, 2014, pp. 1529–1535.
[51] Y. Liao and X. Wang, "Impedance-based stability analysis for interconnected converter systems with open-loop RHP poles," *IEEE Trans. Power Electron.*, vol. 35, no. 4, pp. 4388–4397, Apr. 2020.
[52] Y. Eto, Y. Noge, and M. Shoyama, "A Dynamic characteristic of bi-directional dual active bridge converter with power-feedback control," in *Proc. IEEE 12th Energy Convers. Congr. Expo.-Asia*, 2021, pp. 1940–1945.
[53] A. P. N. Tahim et al., "Modeling and stability analysis of islanded DC microgrids under droop control," *IEEE Trans. Power Electron.*, vol. 30, no. 8, pp. 4597–4607, Aug. 2015.

Yasushi Eto (Student Member, IEEE) received the B.S. degree in system engineering from Hiroshima University, Hiroshima, Japan, in 2019, the M.S. degrees in electrical engineering, in 2021, from Kyushu University, Fukuoka, Japan, where he is currently working toward the Ph.D. degree in electrical and electronics with the Graduate School of Information Science and Electrical Engineering, Kyushu University, Fukuoka, Japan.

His research interests include control and stability of dc–dc converter and dc distribution system.

Mr. Eto is a Member of the Institute of Electrical Engineers of Japan.

Yuichi Noge (Member, IEEE) received the B.S., M.S., and Dr.Eng. degrees in electrical, electronics, and information engineering from the Nagaoka University of Technology, Niigata, Japan, in 2009, 2011, and 2014, respectively.

He joined as a Research Associate with the Monozukuri Engineering Department, Tokyo Metropolitan College of Industrial Technology, Tokyo, Japan, since 2014, and the Institute of Engineering, Tokyo University of Agriculture and Technology, Fuchu, Japan, since 2017. Since 2020, he has been with the Department of Electrical Engineering, Faculty of Information Science and Electrical Engineering, Kyushu University, Fukuoka, Japan. His research interests include the multilevel power conversion circuit, power semiconductor application especially for the active gate driver, and high frequency circuit integration.

Dr. Noge is a Member of the Institute of Electrical Engineers of Japan.

Masahito Shoyama (Senior Member, IEEE) received the B.S. degree in electrical engineering and the Dr.Eng. degree in electronics from Kyushu University, Fukuoka, Japan, in 1981 and 1986, respectively.

In 1986, he joined as a Research Associate with the Department of Electronics, Kyushu University, where he has been an Associate Professor, since 1990, and a Professor, since 2010. Since 2009, he has been with the Department of Electrical Engineering, Faculty of Information Science and Electrical Engineering, Kyushu University. His research interests include the field of power electronics, especially in the areas of bidirectional converters for dc/ac power systems, high-frequency switching converters for renewable energy sources, power factor correction converters, and electromagnetic compatibility.

Prof. Shoyama is a Member of the Institute of Electronics, Information and Communication Engineers, Institute of Electrical Engineers of Japan, and Society of Instrument and Control Engineers.

Tadatoshi Babasaki received the Ph.D degree in system science from Nagasaki University, Nagasaki, Japan, in 2011.

He joined NTT Facilities, Tokyo, Japan, in 2014. He is currently engaged in the energy saving technique of buildings with P.E.Jp (Electrical & Electronics Engineering, Engineering Management). He joined Nippon Telegraph and telephone corporation, Tokyo, in 1990. He has been engaged mainly in development of the dc power feeding system and battery for telecommunication. He engaged in development and standardization of the high voltage dc power feeding system, from 2008 to 2013.